Structural Engineering and Mechanics, *Vol. 74, No. 6 (2020) 723-735*
DOI: https://doi.org/10.12989/sem.2020.74.6.723

Numerical modeling and prediction of adhesion failure of adhesively bonded composite T-Joint structure

Subhransu K Panda[1a], Pradeep K Mishra[1b] and Subrata K Panda[*2]

[1]*Department of Mechanical Engineering, Centre for Advanced Post Graduate Studies, BPUT-769004, Rourkela, Odisha, India*
[2]*Department of Mechanical Engineering, NIT Rourkela, Rourkela-769008, Odisha, India*

(Received December 3, 2019, Revised January 17, 2020, Accepted January 19, 2020)

Abstract. This study is reported the adhesion failure in adhesive bonded composite and specifically for the T-joint structure. Three-dimensional finite element analysis has been performed using a commercial tool and the necessary outcomes are obtained via an eight noded solid element (Solid 185-element) from the library of ANSYS. The structural analysis input has been incurred through ANSYS parametric design language (APDL) code. The normal and shear stress distributions along different layers of the joint structure have been evaluated as the final outcomes. Based on the stress distributions, failure location in the composite joint structure has been identified by using the Tsai-Wu stress failure criterion. It has been found that the failure index is maximum at the interface between flange and web part of the joint (top layer) which indicates the probable location of failure initiation. This kind of failures are considered as adhesion failure and the failure propagation is governed by strain energy release rate (SERR) of fracture mechanics. The different adhesion failure lengths are also considered at the failure location to calculate the SERR values i.e. mode I fracture (opening), mode II fracture (sliding) and mode III fracture (tearing) along the failure front. Also, virtual crack closure technique (VCCT) principle of fracture mechanics steps is used to calculate the above said SERRs. It is found that the mode I SERR is more dominating compared to other two modes of failure for the joint considered. Finally, the influences of various parametric (geometrical and material) effect on SERR of the joint structure are evaluated and discussed in details.

Keywords: adhesion; delamination; failure index; SERR; T-joint; Tsai-Wu criterion; VCCT principle

1. Introduction

Enhanced impact behaviour, the capability to absorb energy, resistance to free vibration and good air tightness are some of the important characteristics provided by the adhesive bonding to the joint structures (Campilho *et al.* 2018). Due to these characteristics as well as with sound deadening and keeping integrity with the material capabilities, bonded structures are commonly used in aerospace industries. In joint structures, the joints are the locations where a structure starts to fail. Joints are mainly classified into two types i.e. in-plane joints and out-of-plane joints. Single lap joint, double lap joint, butt joints come under the in-plane joint category, while T-joint structure generally comes under out-of-plane joints.

T-joint structures are generally bolted or adhesively bonded. Adhesively bonded T-joints are used frequently as it provides uniform strength throughout the joint (i.e. the stress is uniformly distributed). In a composite structure, adhesive joints are not the only weakest link; crack formation between the layers of the laminated structures may cause the failure. This interfacial cracking in between the layers of the laminated composite structure is termed as adhesion/delamination failure.

In general, the applications of T-joint structures can be found in various high performance structural applications in industries like space, aircraft, naval, automobile, and defense industries. So, it is important to understand the failure occurring in the structures. In recent years, due to its wide range of applications, it attracted many researchers to study about it. Composite laminates are the combination of plies/lamina. Delamination/adhesion failure mainly occurs between these plies of the structure when they separate from each other. These kinds of failure is difficult to identify and can do serious damage to any laminated composite structure. Therefore, it is important to know the durability as well as the damage tolerance of the composite laminates.

The fracture mechanics method is generally used to calculate the strain energy release rate of the composite structures. Fracture mechanics is the subject of study, wherein the material's resistance to fracture is described. Crack propagation can be steady (i.e. slowly increasing crack length with time or load) or can be catastrophic (unsteady crack propagation), leading to sudden failure of the material. The virtual crack technique (VCCT) including the finite element method (FEM) have been employed for the analysis of the weakly bonded composite structures. Similarly, a series of research articles are already published on the adhesive bonded composite structures including the failure conditions. Some of the relevant literature on the adhesively bonded joints are discussed in the following

*Corresponding author, Associate Professor
E-mail: pandask@nitrkl.ac.in; call2subrat@gmail.com
[a] Research Scholar
E-mail: subhransupanda3@gmail.com
[b] Assistant Professor
E-mail: capgs.pkmishra@bput.ac.in

ISSN: 1225-4568 (Print), 1598-6217 (Online)

paragraph to show the necessity of the present research.

Elhannani *et al*. (2016) carried out three dimensional (3D) nonlinear finite element (FE) analysis for the evaluation of the stress distribution data for the simple lap joint of variable geometrical parameters. The progressive damage of the single-lap bolted composite joint was investigated by Kapidžić *et al*. (2014) using 3D technique and predicted the fastener forces due to the temperature difference of the hybrid structures. Mokhtari *et al*. (2017) examined the dynamic behaviour of the sandwich T-joint numerically and the result accuracy checked using the experimental data. In addition, a few researchers utilized extended finite element method (E-FEM) for the adhesively bonded structures.

Additionally, various kinematic theories have been proposed to compute the composite structural responses (static and dynamic) of types of components (beams, plates, and shells) under the effect of individual/combined loading i.e. mechanical and thermo-mechanical (Abualnour *et al*. 2019, Belbachir *et al*. 2019, Sahla *et al*. 2019, Bourada *et al*. 2019, Mahmoud and Tounsi 2019, Medani *et al*. 2019, Khiloun *et al*. 2019, Draoui *et al*. 2019, Addou *et al*. 2019, Chaabane *et al*. 2019, Boulefrakh *et al*. 2019, Boukhlif *et al*. 2019, Tlidji *et al*. 2019, Zaoui *et al*. 2019, Zarga *et al*. 2019, Mahmoudi *et al*. 2019, Hussain *et al*. 2019, Meksi *et al*. 2019, Hellal *et al*. 2019, Adda Bedia *et al*. 2019, Semmah *et al*. 2019, Draiche *et al*. 2019, Berghouti *et al*. 2019, Batou *et al*. 2019, Karami *et al*. 2019a, Karami *et al*. 2019b, Karami *et al*. 2019c, Karami *et al*. 2019d, Karami *et al*. 2019e, Alimirzaei *et al*. 2019).

Vosoughi (2015) utilized the concept of Euler-Bernoulli beam theory including the fracture mechanics steps for the identification of cracks in beam component. Perić *et al*. (2014) reported numerically the displacement and the residual stress data of the composite structure considering the effect of temperature. The research concluded that the implementation of 3D shell element reduces 42% of time for the analysis. Prashob *et al*. (2017a) analysed the tubular T-joint numerically via simulation software (ANSYS) and validated with experimental results under the compressive loading. Budhe *et al*. (2017) reviewed the recent developments in adhesively bonded composite joint structures.

Mahieddine *et al*. (2015) developed a finite element model to study the behaviour of partially delaminated layers by using the 1st order shear deformation theory and lateral strain principle. They evaluated the performance of the layers under static and dynamic conditions. Prashob *et al*. (2017b) reviewed the enhancement of strength of steel and concrete structures with the use of carbon fibre reinforced polymer (CFRP) and glass-fibre-reinforced polymer (GFRP) including fibre-reinforced polymers (FRP) for bridge structures. Jayatilake *et al*. (2016) developed three dimensional finite element model to understand the behaviour of free vibration on fiber composites sandwich panels having interlayer delamination. They found that the size of the delamination is an important factor for creating damage in a composite laminate and the dynamic performance can be improved by bolting at the delaminated area. Benchiha and Madani (2015) evaluated the shear stress distribution in a single lap bonded joint using the finite element method. The joint is adhesively bonded using two 2024-T3 aluminium plates. The shear stress is present at the free edge of the bonded region and is maximum near the defect because of high stress concentration. Gulasik and Coker (2014) have performed two dimensional finite element analysis to understand the delamination of a co-bonded composite T-joint structure and analysis was carried out by applying pull load at 0° using finite element software ABAQUS. Nimje and Panigrahi (2015) have performed a three dimensional nonlinear finite element analysis to study the behaviour of double supported adhesively bonded composite T-joint structure having interfacial failure embedded with it. The adhesion failure initiation and its propagation along the crack front reported by Mishra *et al*. (2016) for spar wing-skin joint (SWJ) using the fracture mechanics approach. The SERRs showed an increasing trend with increase in the adhesion failure length. Rybicki and Kanninen (1977) used a crack closure technique to calculate stress intensity factor and the stress distribution in composite joint structure.

In the above mentioned literatures, it is found that 3D FEM coupled with fracture mechanics approach has been generally adopted for the failure analysis of different adhesively bonded composite joint structures. However, study relevant to the T-type composite joint structures with adhesion/delamination failure is limited. Further, failure location identification and propagation studies of T-joints subjected to out of plane loadings are complex in nature. Hence, in the present study, a 3D FE modeling has been carried out for the adhesive bonded composite T-joint structure subjected to out-of-plane loading to evaluate the normal and shear stress distributions at different locations. Failure locations of the joint structure have been found out by using Tsai-Wu failure criteria. Accordingly, various modes of SERRs have been calculated at the identified failure locations by considering different failure lengths. Additionally, the efficacy of the joint structure has been analyzed by conducting various parametric studies of the T-joint structure for different material properties, laminated orientation scheme, number of layers, thickness and fillet supports etc.

2. FE modelling of adhesively bonded composite T-joint

The geometry of adhesively bonded composite T-joint structure along with its dimensions are shown in Fig. 1 and Table 1. The layered material modeled using Solid 185 type of element from ANSYS FE package. The material properties of the laminated joint structure used are given in Table 2 and 3. Each web and flange laminate is made up of four layers with orientation scheme [0/90/90/0]s.

Accuracy and efficiency of finite element method software depends upon the meshing size of the model (Madenci and Guven 2015). A very fine mesh (convergence) is adopted to design the model so that the results would be more accurate i.e. 0.001% error in normal and shear stresses. In the present study, the model is

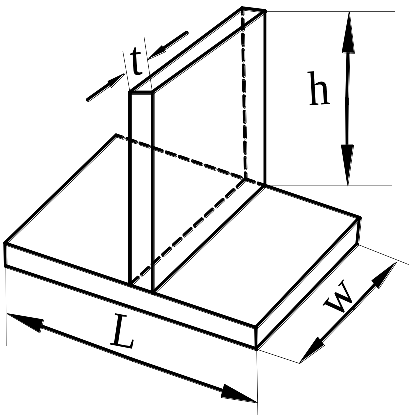

Fig. 1 Representation of adhesive bonded T-joint

Table 1 Dimensions of the adhesive bonded T-joint

Length (L) in meter	0.16
Width (w) in meter	0.18
Height (h) in meter	0.16
Thickness (t) in meter	0.0025

Table 2 Elastic properties of T300/934 carbon epoxy plain ply (Cheuk and Tong 2002)

In-plane Elastic moduli, E_x and E_y (GPa)	57.226
Transverse modulus, E_z (GPa)	4.800
In-plane shear modulus, G_{xy} (GPa)	4.481
Out-of-plane shear moduli, G_{yz}, G_{xz} (GPa)	4.400
In-plane Poisson's ratio, ν_{xy}	0.050
Out-of-plane Poisson's ratios, ν_{xz}, ν_{yz}	0.280

discretized into 2080 elements, which are a combination of 4662 nodes as shown in Fig. 2. Fig. 3 depicts the loading and boundary conditions of the joint structure i.e. bottom left edge of the flange part in the joint structure is assumed to be fixed in all directions (DOF = 0) and the top nodes of the web part is subjected to out-of-plane load (P_y) of 100N (Li *et al*. 1997).

3. Three dimensional stress analysis of adhesively bonded T-joint structure

Three dimensional stress analysis of the composite T-joint structure has been evaluated using the finite element method. The normal and shear stress components (σ_{xx}, σ_{yy}, σ_{zz}, σ_{xy}, σ_{yz}, σ_{zx}) in all layers of the laminated T-joint structure are being calculated and shown in Fig. 4 and Fig. 5. The stress distribution shows similar trends in all layers but more significant at the top two layers of the joint structure. Fig. 4 shows the distribution of stress in the bonded layer of the flange and web part and Fig. 5 shows the stress distribution in the 1st layer (below the bonded layer). It is observed that the stress induced in the y-direction (σ_{yy}), is more dominant compared to all other stress components and maximum at the bonded region of the flange and web part of the joint structure.

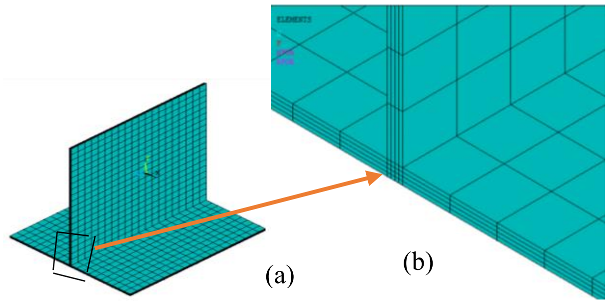

Fig. 2 (a) Meshed view and (b) zoomed view of the T-joint structure

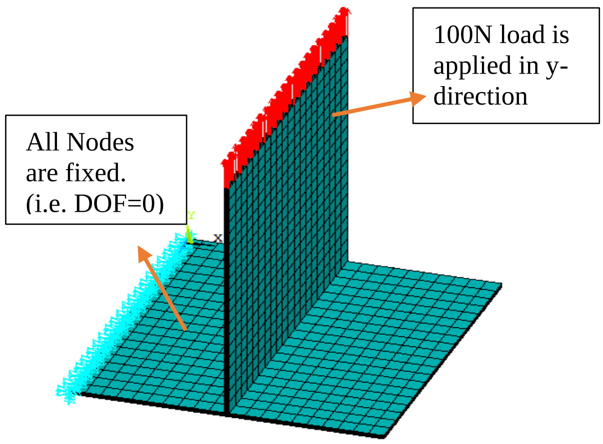

Fig. 3 Boundary condition of T-joint structure

Table 3 Mechanical strength of T300/934 carbon epoxy plain ply (Cheuk and Tong 2002)

Longitudinal tensile strength, X_t (MPa)	1270.0
Longitudinal compressive strength, X_c (MPa)	1130.0
In-plane tensile strength, Y_t (MPa)	42.0
In-plane compressive strength, Y_c (MPa)	141.0
Inter-laminar normal strength, Z (MPa)	46.0
Inter-laminar shear strength, S (MPa)	90.0

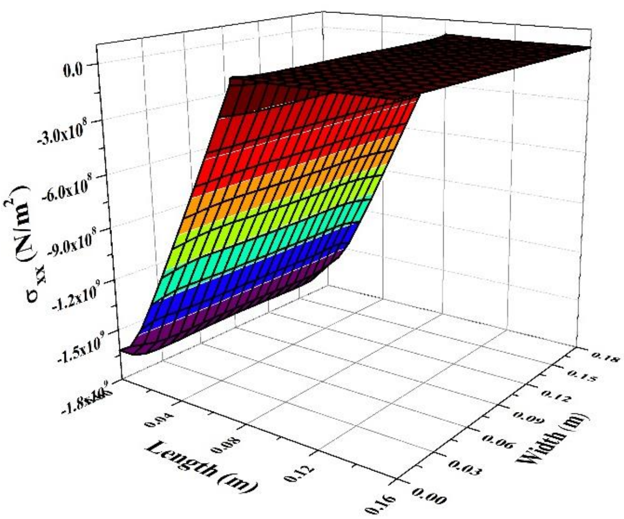

(a) Distribution of normal stress in x-direction (σ_{xx})

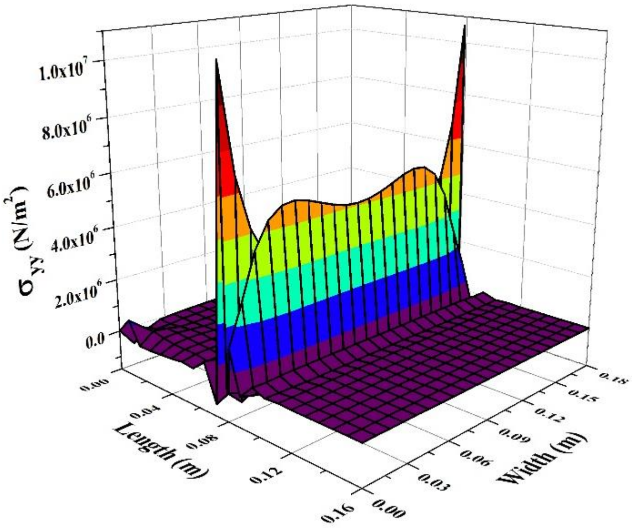

(b) Distribution of normal stress in y-direction (σ_{yy})

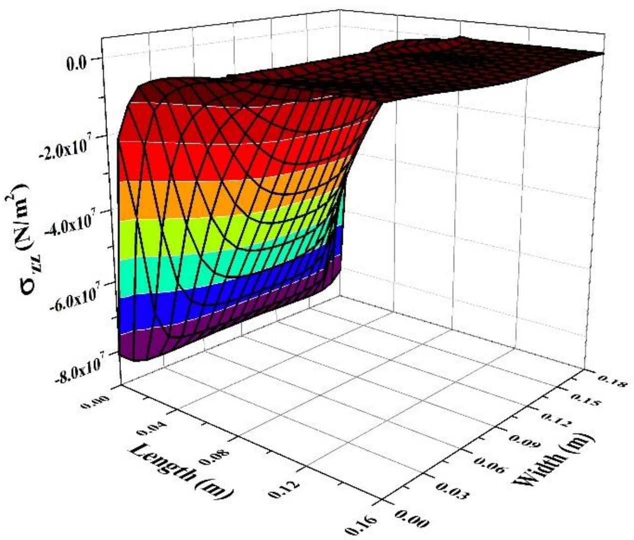

(c) Distribution of normal stress in z-direction (σ_{zz})

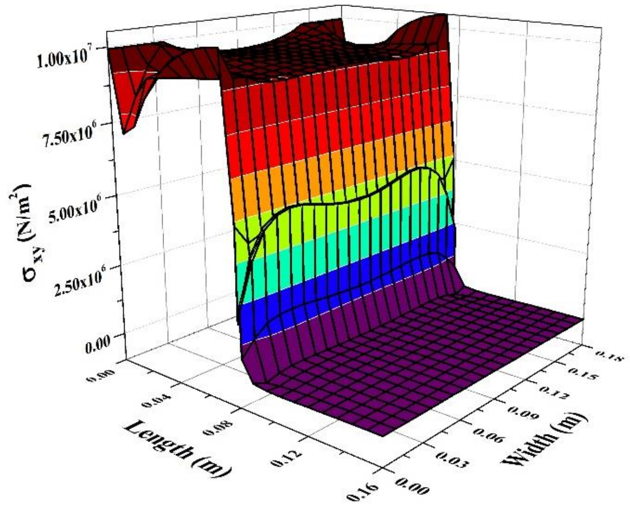

(d) Distribution of shear stress in xy-direction (σ_{xy})

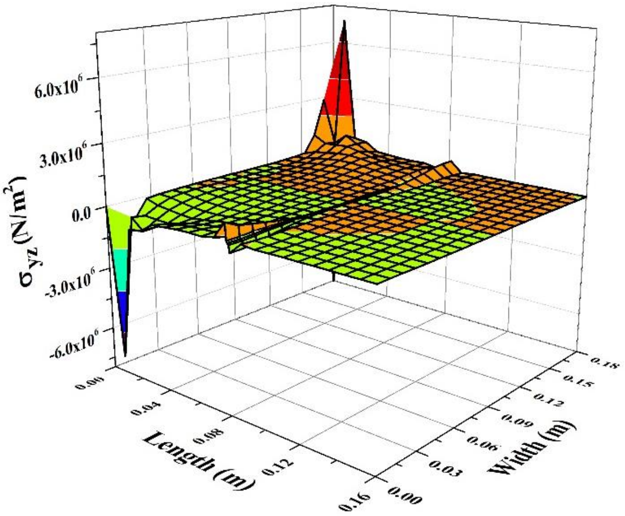

(e) Distribution of shear stress in yz-direction (σ_{yz})

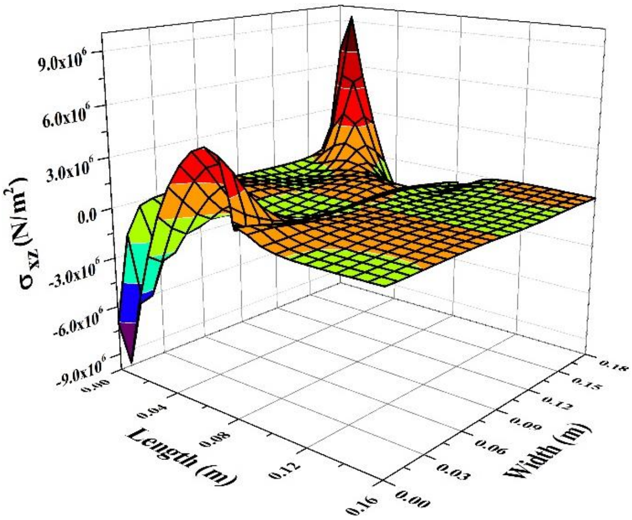

(f) Distribution of shear stress in xz-direction (σ_{xz})

Fig. 4 Stress distributions of the T- joint structure (Top layer of flange)

4. Identification of failure location in the T- joint structure

In general, three types of failure occur in adhesively bonded joint structures:

- Cohesive failure, occurs within the adhesive.
- Interfacial or adhesive failure, generally occur between the adhesive and the adherend.

Inter-laminar failure known as delamination, which occurs within the adherend.

Three dimensional stress analysis has been carried out to investigate the damages over the surfaces of the composite T-joint structure subjected to out-of-plane loading. The failure initiation location can be identified by using these stresses along with their strength values. Tsai–Wu quadratic failure criterion (Tsai, 2018) given in Equation (1) have been used taking both normal and shear stress components to calculate the failure occurred in the T-joint structure.

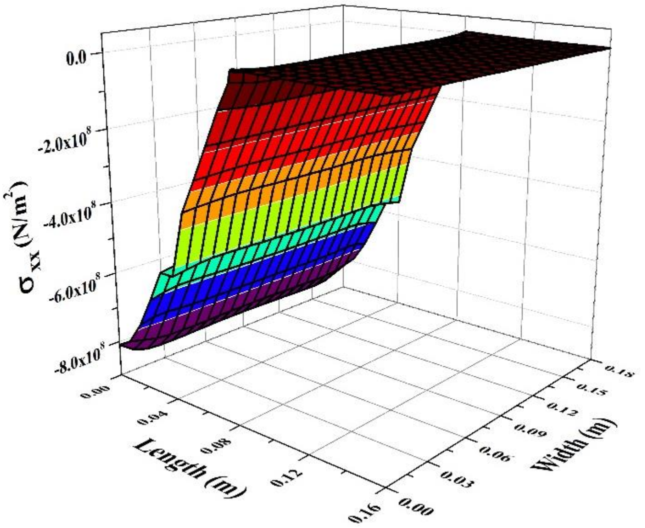

(a) Distribution of normal stress in x-direction (σ_{xx})

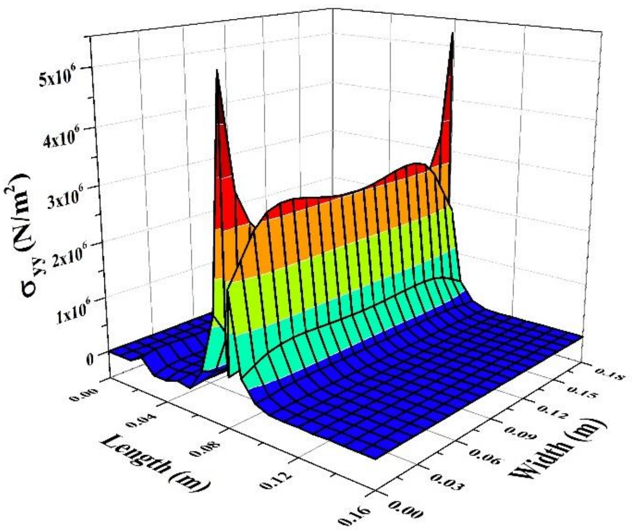

(b) Distribution of normal stress in y-direction (σ_{yy})

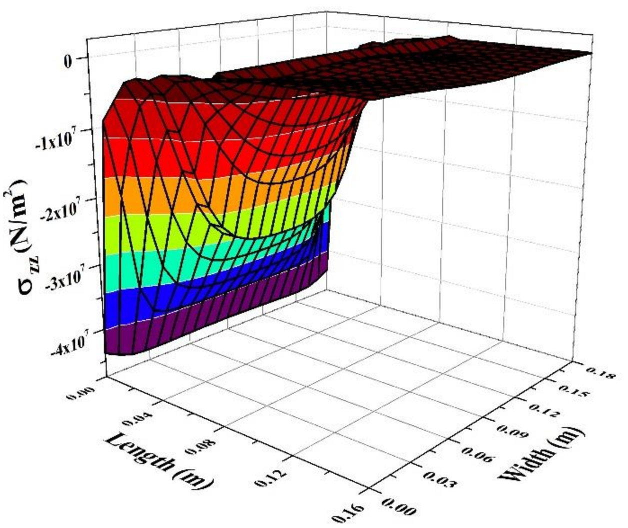

(c) Distribution of normal stress in z-direction (σ_{zz})

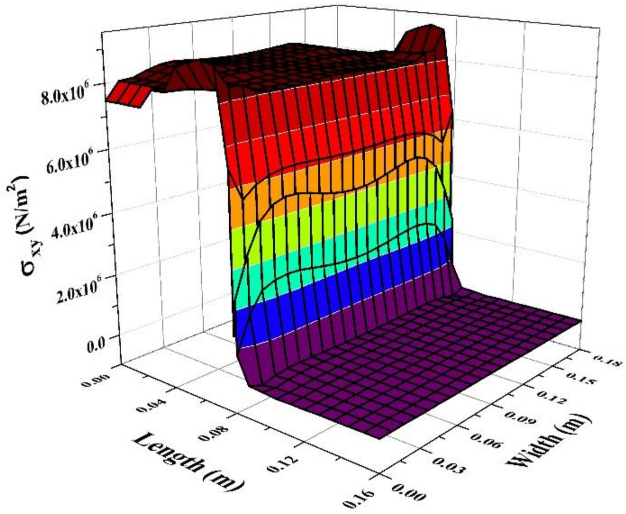

(d) Distribution of shear stress in xy-direction (σ_{xy})

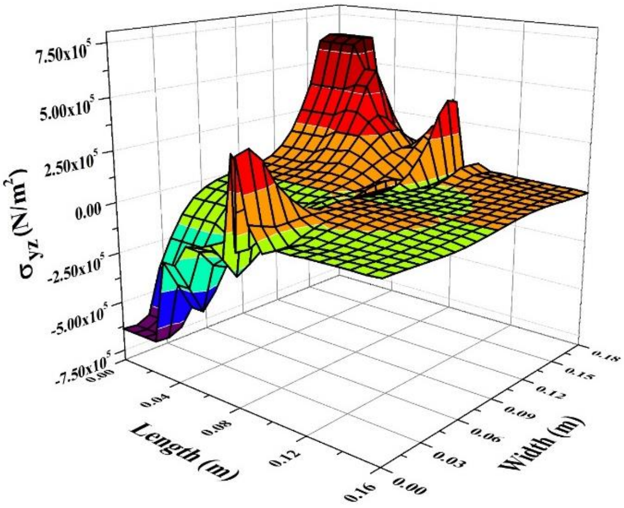

(e) Distribution of shear stress in yz-direction (σ_{yz})

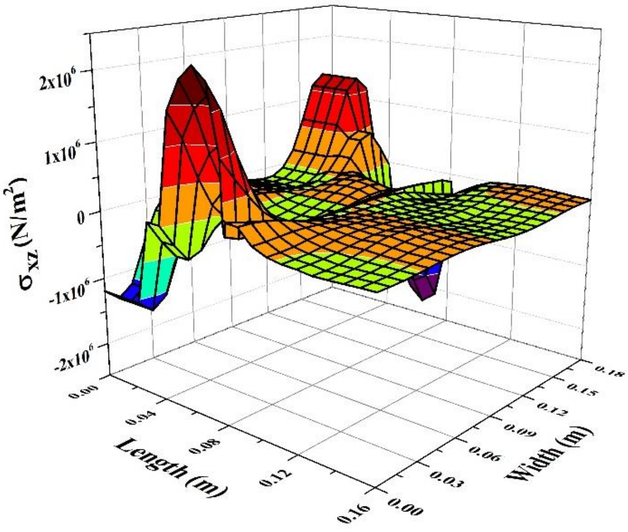

(f) Distribution of shear stress in xz-direction (σ_{xz})

Fig. 5 Stress distributions of the T-joint structure (2nd layer of flange)

$$\frac{\sigma_x^2}{X_cX_t}+\frac{\sigma_y^2}{Y_cY_t}+\frac{\sigma_z^2}{Z_cZ_t}+\frac{\tau_{xy}^2}{S_{xy}^2}+\frac{\tau_{yz}^2}{S_{yz}^2}+\frac{\tau_{xz}^2}{S_{xz}^2}+\sigma_x\left(\frac{1}{X_t}-\frac{1}{X_c}\right)$$
$$+\sigma_y\left(\frac{1}{Y_t}-\frac{1}{Y_c}\right)+\sigma_z\left(\frac{1}{Z_t}-\frac{1}{Z_c}\right)+f_{xy}\sigma_x\sigma_y+f_{yz}\sigma_x\sigma_y \quad (1)$$
$$+f_{xz}\sigma_x\sigma_y = e^2\begin{cases} e<1, & \text{no failure} \\ e\geq 1, & \text{failure}\end{cases}$$

Here, X_t, X_c and Z_t are the allowable tensile strengths in the three principal directions of the material and S_{xy}, S_{yz} and S_{xz} are the shearing strengths in different coupling modes of the orthotropic layer. Similarly f_{xy}, f_{yz} and f_{xz} are the coupling co-efficient along X, Y and Z directions.

Here, the T-joint structure is subjected to out-of-plane load in the y-direction. So, the damage initiation can be predicted by the normal stress component in y-direction (σ_y) and the inter-laminar shear stress components (τ_{xy},τ_{yz}). Therefore, the Tsai-Wu stress criterion as given in Equation (1) is reduced to the following equation.

$$(\frac{\sigma_Y}{Z})^2+(\frac{\tau_{xy}}{S})^2+(\frac{\tau_{yz}}{S})^2=e^2\begin{cases} e<1, \text{no failure} \\ e\geq 1, \quad \text{failure}\end{cases} \quad (2)$$

Where Z is the inter-laminar normal strength and S is the inter-laminar shear strengths which are considered to be equal (i.e. $S_{xy} = S_{yz} = S$).

Using the Tsai-Wu stress criterion given in Equation (2) the failure index has been evaluated for all four layers of the laminated T-joint structure. The failure index in the bonded layer (1st layer of the flange) of the flange and web part and layer below to this has been found to be pre-dominant. Therefore, the failure index for these two layers has been plotted in Figs. 6 and 7. Among these two, the failure index has been found to be pre-dominant for the top layer of the joint structure as shown in Fig. 6. Therefore, adhesion failure is the reason behind the damage occurring in the T-joint structure considered in the present case. Fig. 7 shows the failure index in the layer below the top surface for the failure of the joint structure.

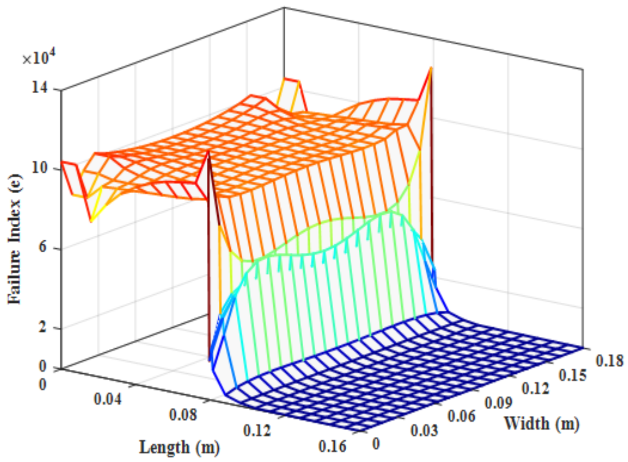

Fig. 6 Distribution of failure index for the top layer of the flange part

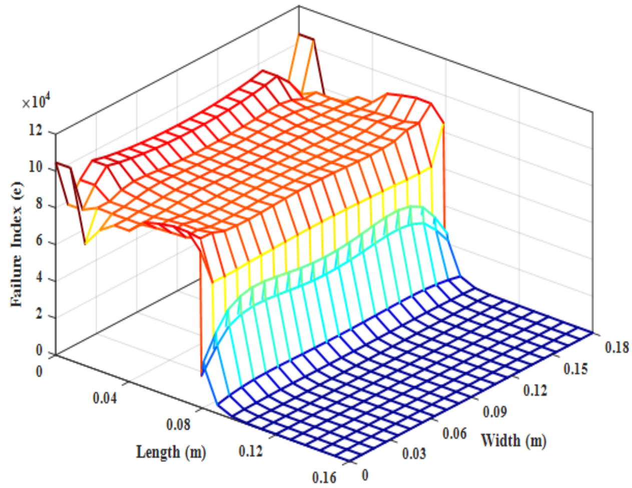

Fig. 7 Distribution of failure index for the 2nd layer of the flange part

5. Adhesion failure propagation of the joint structure

From the previous section, the failure location of the joint structure has been identified and found to be at the top layer of the flange part. Hence, adhesion failure has been embedded in the joint structure and the failure/damage propagation has been evaluated using the SERRs.

Virtual crack closure technique (VCCT) of fracture mechanics has been used to calculate the SEERs along the failure front. The schematic diagram of the adhesively bonded T-joint structure embedded with adhesive failure length (c) has been shown in Fig. 8. The failure analysis of the joint structure has been carried out for three different failure lengths present at a distance of 0.0006 m, 0.0012 m and 0.0018 m from left end of the web. The SERRs for all modes (G_I, G_{II}, G_{III}) have been calculated at the adhesion failure locations along the failure front. The behaviour of the adhesion failure along the failure front can be visualized from the variation of SERRs.

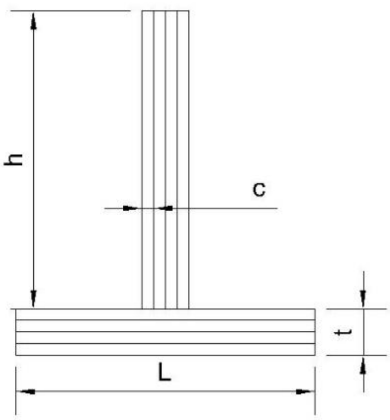

Fig. 8 Schematic diagram of adhesive bonded T-joint structure with embedded adhesive failure length (c), m

5.1 Calculation of SERRs

Figure 8 represents the schematic diagram of the T-joint structure with initial adhesion failure length 'c' embedded along the width of the structure. The crack can be closed by calculating the nodal forces along the crack front. These nodal forces can be calculated using Multipoint constraint

(MPC) elements. Then, the VCCT principle which is based on Irwin's crack closure method (Irwin 1957) used to calculate the SERRs. According to Irwin's crack closure method, the amount of energy required to close the crack is identical to the amount of energy released during the crack propagation. As shown in Fig. 9 the crack tip is propagated from c (Fig. 9 (a)) to '$c+\Delta c$' (Fig. 9 (b)) and closed between the point i and f. Equation (3) represents the amount of energy required to close the crack tip along one side of the element for a two dimensional four-noded element structure as shown in Fig. 9(a) and 9(b).

$$\Delta E = \frac{1}{2}(X_{1i}.\Delta u_{2i} + Z_{1i}.\Delta w_{2i}) \qquad (3)$$

where, X_{1i} and Z_{1i} represent the nodal forces at point i for shear and opening mode as shown in Fig. 9 (a). Similarly, Δu_{2i}andΔw_{2i} represent the difference of nodal displacements in shear and opening mode at node i as shown in Fig. 9 (b).

Conditions are established in Irwin's crack closure method before the propagation of the crack. This method establishes the original condition before the crack was extended. For that reason, the forces acting at the upper and lower surfaces of the closed cracks will be equal to the forces required to close the cracks. In one Finite element analysis can be used for the closed crack to evaluate the forces X_{1i} and Z_{1i}. Similarly, in second finite element analysis the displacement values Δu_{2i} and Δw_{2i} for the extended crack to length '$c+\Delta c$' can be calculated as shown in Fig. (b). 3D VCCT with eight-noded solid elements is shown in Fig. 9 (c) which is used for the present calculations.

5.2 VCCT Method

The nodal forces obtained at the node point of the finite element model along the failure plane, when multiplied with the face displacements due to adhesion failure along the failure plane will give the energy based stress equation (Rybicki and Kanninan 1977).

According to VCCT principle, the SERRs for different modes of failure and the total SERR can be calculated from the following equations:

$$G_I = \frac{1}{2\Delta A} Z_f(u_T - u_B) \qquad (4)$$

$$G_{II} = \frac{1}{2\Delta A} X_f(w_T - w_B) \qquad (5)$$

$$G_{III} = \frac{1}{2\Delta A} Y_f(v_T - v_B) \qquad (6)$$

$$G_T = G_I + G_{II} + G_{III} \qquad (7)$$

where, the virtually closed area (ΔA) = $\Delta c \times \Delta c$ and Z_f, X_f and Y_f are the opening, sliding and tearing mode forces, respectively. These forces are required for adhesion failure growth. The MPC elements are used for evaluation of these forces. G_I, G_{II} and G_{III} are calculated for varying

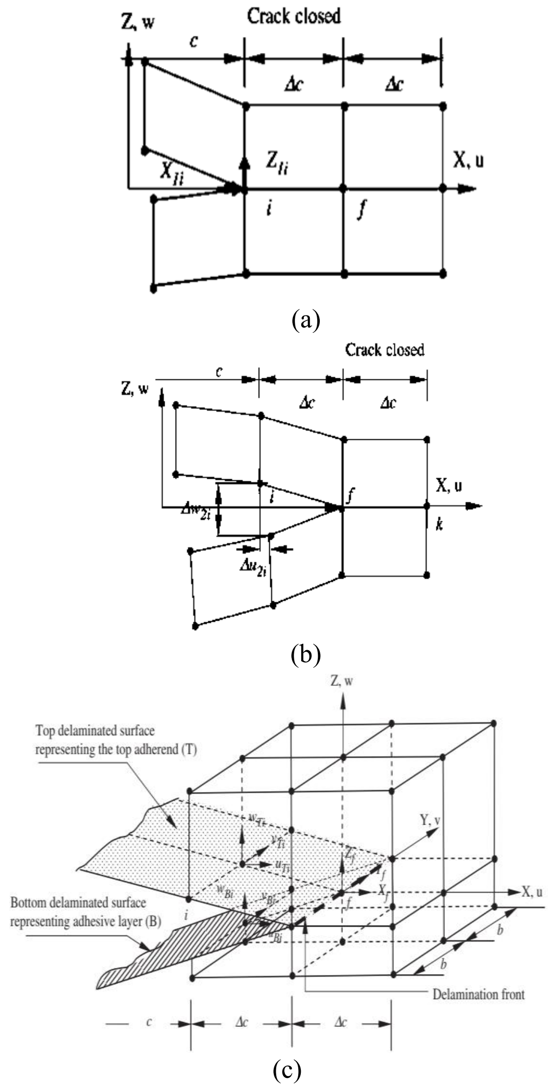

Fig. 9 2D crack closure method: (a) 1st step – crack closed and (b) 2nd step – extended crack length (c) 3D VCCT with eight-noded solid elements

values of 'c'. The rate of variation of these values would characterize the adhesion failure growth. Thus, the three components of SERR have been computed using the VCCT method in the present analyses.

6. Results and discussion

6.1 Validation study

For the validation and comparison study, strain energy release rate (SERR) for mode I failure of the lap joint structure (Panigrahi and Pradhan 2007) has been analysed. The SERRs are taken along the delamination front at the crack length of 0.5 mm of the lap joint structure. The lap joint is subjected to displacement in the x-direction in the top adherend whereas the bottom adherend is fixed from one end. The geometry and material properties are the same as that of reference (Panigrahi and Pradhan 2007). It is found that the result of the present FE analysis shows good agreement with the available literature as shown in Fig. 10.

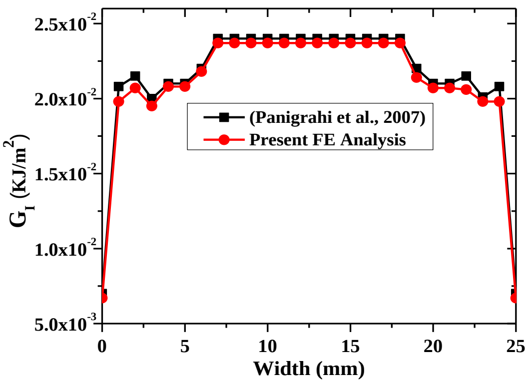

Fig. 10 Comparison of G_I between present FE analysis and (Panigrahi *et al*. 2007)

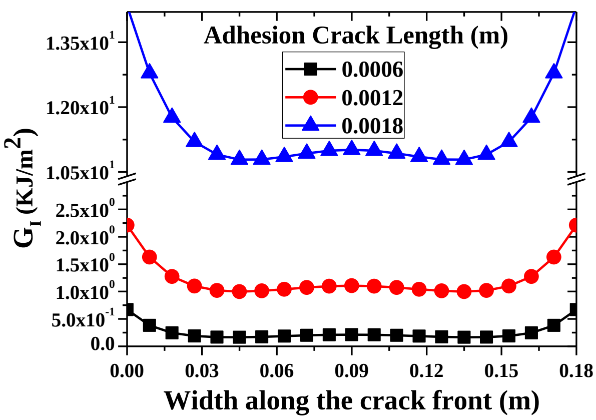

(a) SERRs for mode I

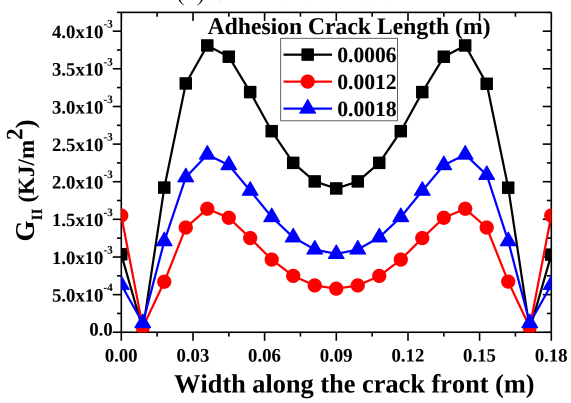

(b) SERRs for mode II

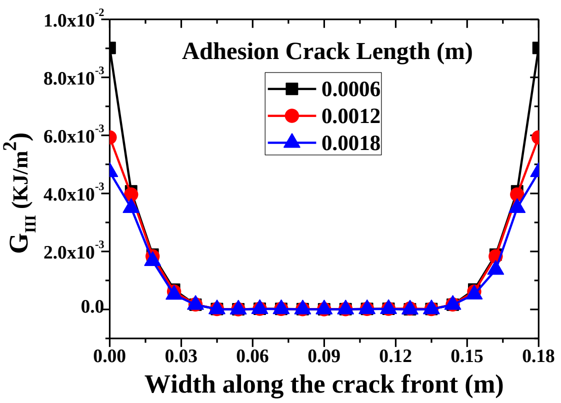

(c) SERRs for mode III

Fig. 11 Distribution of SERRs over various adhesive crack length

6.2 Adhesion failure analysis

Adhesion failure generally occurs between the lamina of a laminated composite structure. Here, the SERRs are calculated at the adhesion crack lengths for all three modes of failure (G_I, G_{II}, G_{III}) along the crack front. Fig. 11 shows the SERRs along the crack front for all three modes of failure. Fig. 11(a) shows the SERRs for mode I failure for all the crack lengths using the material properties, boundary conditions described in Section 2 and 3.

It has been investigated that for mode I failure, as the crack length increases the SERRs also increases and it is found to be maximum at the crack length of 0.0018 m as shown in Fig. 11(a). Here, SERRs are lower at the central region and maximum at the edges and at the central region, the SERRs are approximately constant along the crack front.

Similarly, Fig. 11(b) shows the SERRs variation for mode II type of failure. It demonstrates that the SERRs at the adhesive crack length of 0.0006 m is maximum. Similarly, Fig. 11(c) is plotted for the SERRs of mode III failure and it depicts that the values for all three modes are similar values at all crack lengths. In this case, SERRs are lower at the central region and maximum at the edges. Fig. 12 shows the distribution strain energy release rate for all three modes of failure. It has been found that the SERR for mode I failure is more dominating compared to the other two modes of failure. Since mode I (G_I) is responsible for the propagation of damage due to adhesion failure, this explains the laminated T-joint structure experience opening mode failure. So, it is important to calculate the SERR for mode I (G_I) and total SERR (G_T) to understand the propagation of crack along the crack front. Fig. 13 shows the propagation of total strain energy release rate (G_T) for different crack lengths. It describes that as the adhesive crack length increase the SERR value also increases. This happens as the bonding area between the top and bottom adherend decrease then more amount of strain energy is released.

7. Influence of various parameters on SERRs of adhesive bonded T-Joints

7.1 Variation in SERRs of adhesive bonded T-joint with varied fiber orientation schemes

In this section, SERRs of the laminated T-joint structure have been calculated for different fiber orientation schemes of web and flange. The orientation schemes are unidirectional (0/0/0/0), cross ply symmetric (0/90/90/0) angle ply symmetric (45/-45/-45/45), angle ply asymmetric (45/-45/-45/45), and quasi-isotropic (0/45/-45/90). The SERR values for mode I failure have been found to be more dominating compared to mode II and mode III failure mode. Therefore, SERRs for mode I (G_I) and total SERR (G_T) have been calculated at different failure length.

Table 4 shows the SERR values for different adhesive failure length with various fiber orientations. It is found that SERRs increases with increase in adhesion failure lengths. SERR is maximum for angle ply symmetric and angle

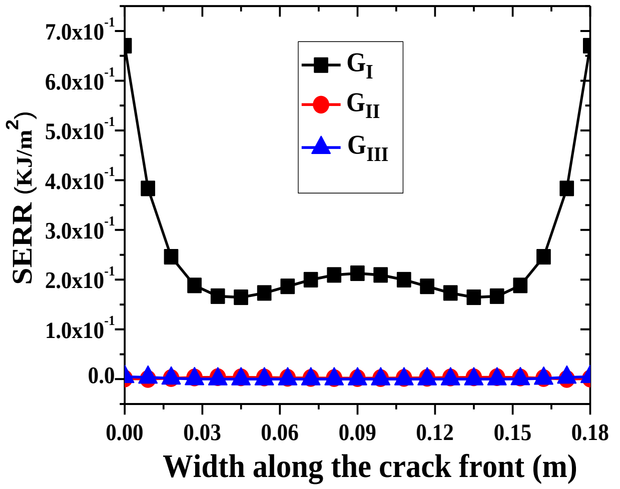

Fig. 12 Distribution of SERR at crack length of 0.0006 m for mode I, mode II and mode III

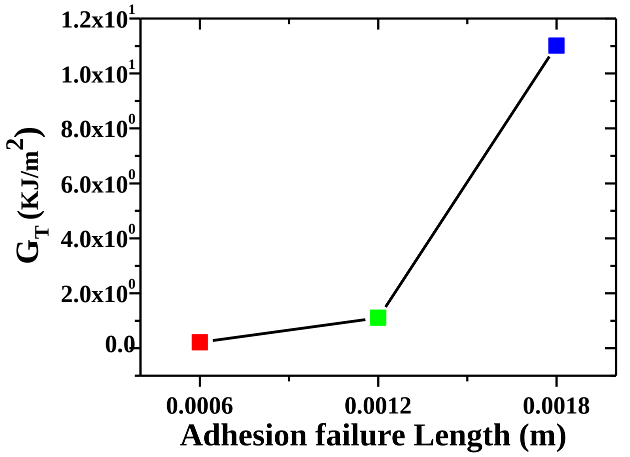

Fig. 13 Variation of total SERR (G_T) along the delamination front

ply asymmetric orientation in the edges of the joint structure. For quasi-isotropic, maximum SERRs observed at the middle of the structure.

7.2 Variation in SERRs of adhesive bonded T-joint with varying laminate material properties

Material properties i.e. Poisson's ratio, strength, stiffness, thermal expansion, moisture expansion, thermal conductivity, and electrical conductivity are described by vector or tensor directional properties. These are functions of orientation in composite anisotropic materials. Fiber composite materials can exhibit various degrees of anisotropy properties.

In this section, the adhesively bonded T-joint structure has been analysed by varying the material properties including the material anisotropy (refer to Table 5) of different fibers. Fig. 14 shows the variation of SERR in mode I (G_I) at the crack length of 0.0006 m. It shows that graphite fiber gives maximum SERR whereas, boron fiber show more resistance to adhesion failure propagation. Similar trends can be spotted for total SERR (G_T) shown in Fig. 15.

Table 4 Distribution of SERR for mode I (G_I) and total SERR (G_T) for different fiber orientation schemes

Adhesion Failure Length (m)	fiber orientation schemes	G_I (J/m^2)	G_T (J/m^2)
	[0/0/0/0]	212.7	214.6
	[0/90/90/0]	212.7	214.6
0.0006	[45/-45/-45/45]	12.4	40.56
	[45/-45/45/-45]	12.4	40.56
	[0/45/-45/90]	211.6	213.8
	[0/0/0/0]	1106.8	1107.3
	[0/90/90/0]	1106.8	1107.3
0.0012	[45/-45/-45/45]	1292.2	1295.3
	[45/-45/45/-45]	1292.2	1295.3
	[0/45/-45/90]	1080.0	1081.0
	[0/0/0/0]	11012.0	11014.0
	[0/90/90/0]	11012.0	11014.0
0.0018	[45/-45/-45/45]	7801.3	7809.4
	[45/-45/45/-45]	7801.3	7809.4
	[0/45/-45/90]	10888.0	10889.0

Table 5 Material anisotropy of different materials (Daniel *et al*. 1994)

	E_1/E_2	E_1/G_{12}
E-glass	4.0	9.5
Boron fiber	9.3	37.4
Carbon fiber	14.2	21.3
Kevlar fiber	14.5	37.0
Graphite fiber	46.0	60.0

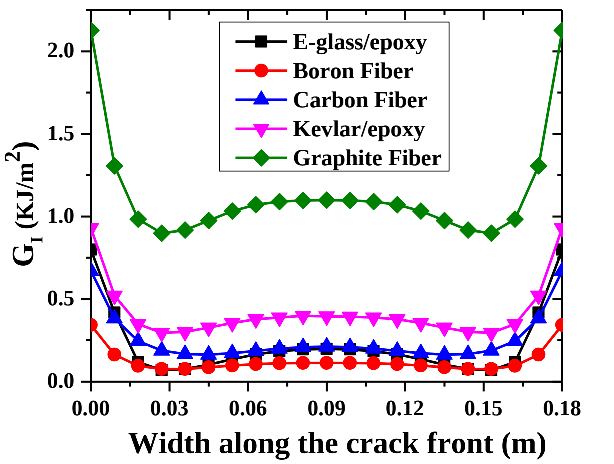

Fig. 14 Distribution of SERR for mode I (G_I) for different material properties

7.3 Variation in SERRs of adhesive bonded T-joint with varied laminate thickness

In this section, the T-joint structure has been analyzed by varying the thickness keeping all other dimensional variables constant. It is found that the SERRs increases with decrease in the thickness of the structure. Fig. 16 shows the

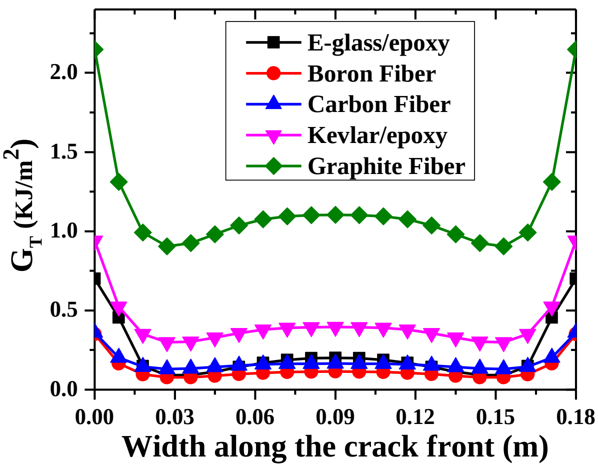

Fig. 15 Distribution of SERR for total SERR (G_T) for different material properties

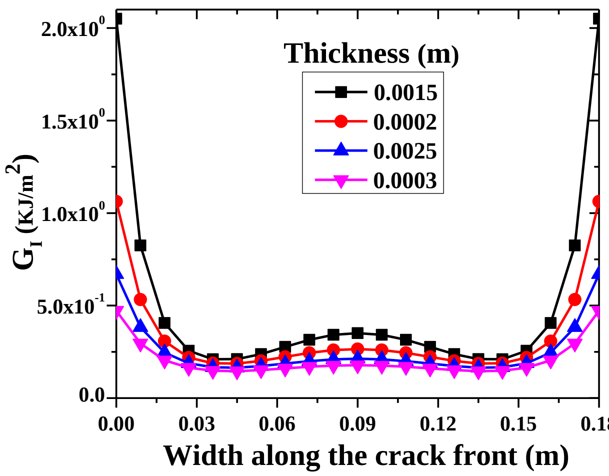

Fig. 16 Distribution of SERR for mode I (G_I) for different thickness

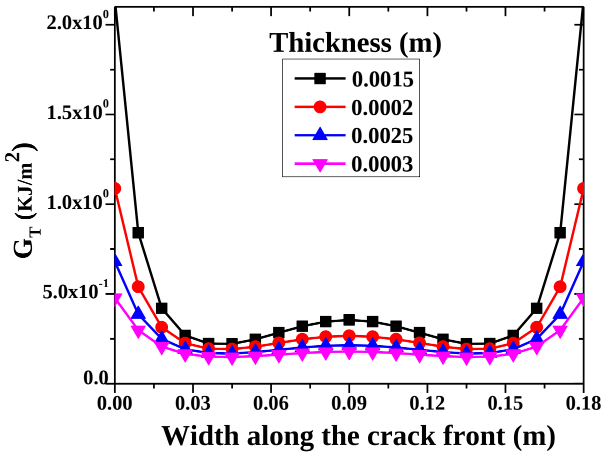

Fig. 17 Distribution of SERR for total SERR (G_T) for different thickness

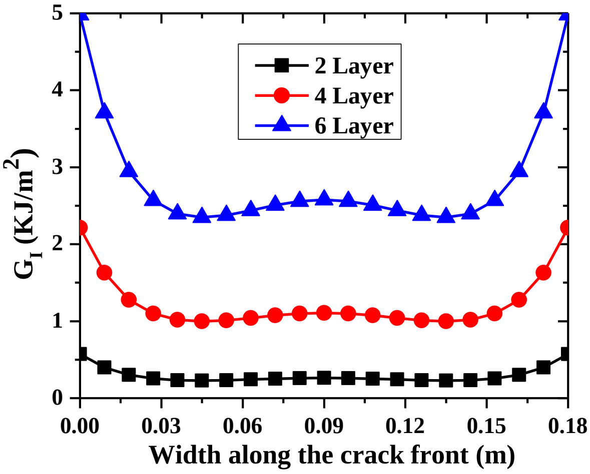

Fig. 18 Distribution of SERR for mode I (G_I) for different number of layers

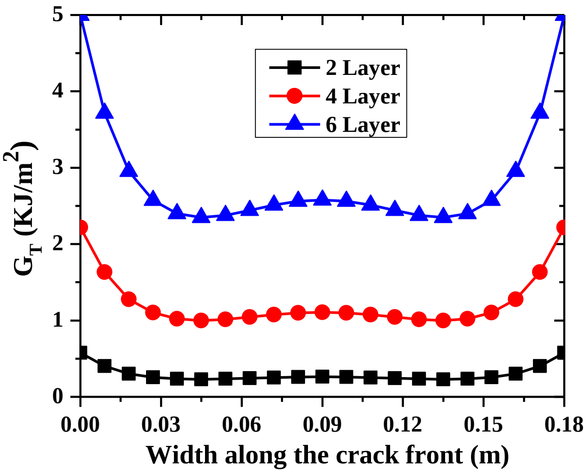

Fig. 19 Distribution of SERR for mode I (G_I) for different number of layers

distribution of SERR for mode I (G_I) failure and total SERRs (G_T) are shown in Fig. 17. As the thickness decreases the contact area between the flange and web part decreases, therefore SERRs increases.

7.4 Variation in SERRs of adhesive bonded T-joint with varied laminate layers

In this section, the influence of the use of a number of layers (plies) on the SERR has been discussed. For this purpose, laminated composite structures having 2 layers, 4 layers, 6 layers and 8 layers laminae have been considered. As the thickness of the individual layer will be different for all the cases, the SERR values at the 0.0012m adhesive failure length has been calculated. It is found that the composite laminated joint structure improves the adhesion failure damage growth resistance as the number of layers decreases. This demonstrates that the SERR values of a laminated composite structure depend on the individual lamina, as the crack is occurring in between them. Fig. 18 and 19 show the distribution of SERR for different layers of the laminated composite structure for mode I and total SERR, respectively.

7.5 Variation in SERRs of adhesive bonded T-joint with fillet support

In this section, the influence of fillet support to the T-joint structure has been analysed. Fig. 20 shows schematic diagram of T-joint structure with both the side fillet supports. The fillet angles have been chosen to be α = 2.5º and 5º. 'G_I' and 'G_T' values have been obtained and shown in Figs. 21 and 22. It is found that with the increase in fillet angles, the SERR values decrease i.e. the joint structure shows more resistance to the damage propagation at α = 5º. This is due to the fillet supports to the web part.

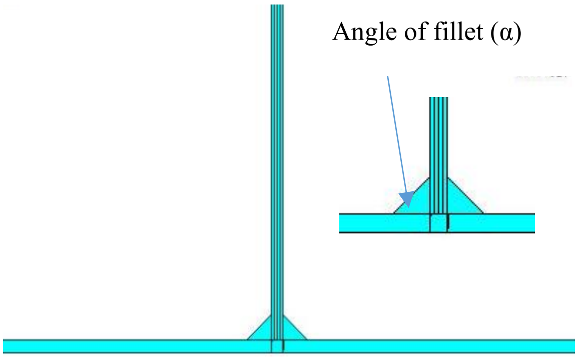

Fig. 20 Schematic diagram of T-joint structure with fillet

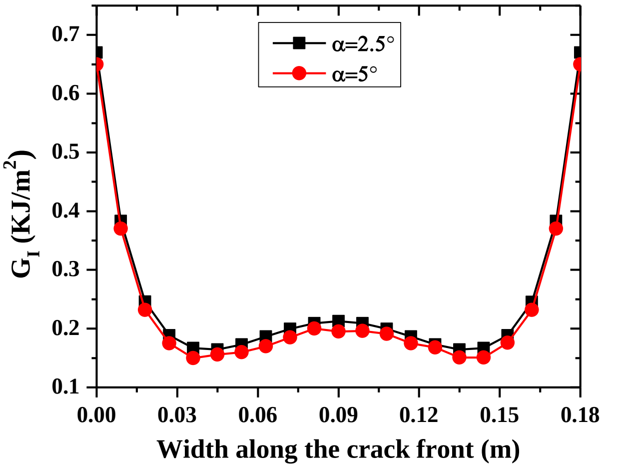

Fig. 21 Distribution of SERR for mode I (GI) for different fillet angle

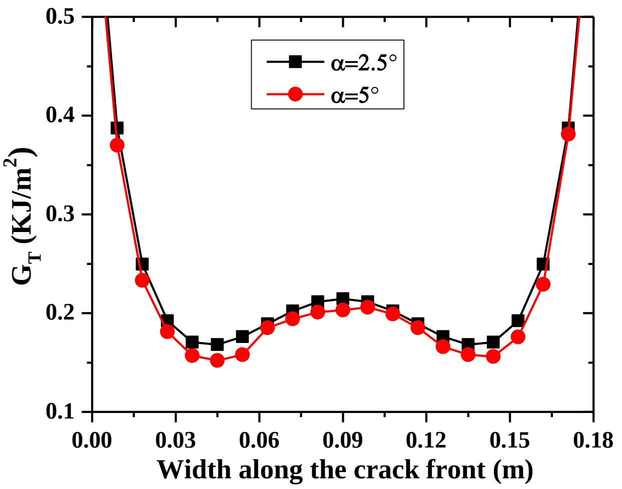

Fig. 22 Distribution of total SERR (G_T) for different fillet angle

8. Conclusion

In this present study, the three-dimension stress analysis and failure analysis have been conducted for the adhesively bonded composite T-joint structure. The stress distribution in both normal and shear planes have been evaluated for all the layers (web and flange) of the laminated structure. Then the failure indices have been calculated by using the Tsai-Wu failure criteria. After the identification of the failure location, the strain energy release rate (SERR) has been calculated by varying the adhesion failure length. The SERR values are obtained for three different crack length (0.0006 m, 0.0012 m and 0.0018 m) along the adhesion failure front using Virtual Crack Closure Technique (VCCT). Then, parametric studies have been conducted for the joint structure by varying the material properties, thickness, orientation scheme, number of laminate layers, and fillet support. The following observations have been obtained from the above analysis:

- It is observed that the out-of-plane stresses induced are higher at the interface region of the flange and web part of the T-joint structure.
- From the failure analysis, it is observed that the failure index is more prominent at the top layer of flange i.e. at the flange and web interface of the T-joint structure compared to other layers. Hence, adhesion failure will occur at this location.
- SERR for mode I adhesion failure is more dominating compared to the other two modes of failure for the joint considered. As all three modes of failure are non-uniform in nature, it is important to calculate the total SERR (G_T) to understand the adhesion failure growth along the failure front. The 'G_T' value increases with increase in adhesion failure length and show a sudden rise after the crack length of 0.0012m.
- It is also observed that with the increase in adhesive failure length the SERR value increases. This happens due to the decrease in the bonding area between the top and bottom adherend of the joint structure resulting release of more amount of strain energy.
- From the 'G_I' and 'G_T' values, it is found that angle ply symmetric and angle ply asymmetric orientation are more suitable for the joint structure considered.
- For the material anisotropy study, it is found that T-joint made up of boron fiber shows more adhesion failure resistance compared to other materials.
- SERR values increase with decrease in the thickness of the structure.
- The adhesion failure resistance of the joint structure increases with the increase in support fillet angle (i.e. α=5º).

References

Abualnour, M., Chikh, A., Hebali, H., Kaci, A., Tounsi, A., Bousahla, A. A. and Tounsi, A. (2019), "Thermomechanical analysis of antisymmetric laminated reinforced composite plates using a new four variable trigonometric refined plate theory", *Comput. Concrete*, **24**(6), 489-498. http://www.technopress.net/index.ph-p/cac/article/view/182.

Adams, R.D. and Peppiatt, N.A. (1974), "Stress analysis of adhesive-bonded lap joints", *J. Strain Analysis*, **9**(3), 185-196. https://doi.org/10.1243/03093247V093185.

Addou, F. Y., Meradjah, M., Bousahla, A. A., Benachour, A., Bourada, F., Tounsi, A. and Mahmoud, S. R. (2019), "Influences of porosity on dynamic response of FG plates resting on Winkler/Pasternak/Kerr foundation using quasi 3D HSDT", *Comput. Concrete*, **24**(4), 347-367. https://doi.org/10.12989/cac.2019.24.4.347.

Alimirzaei, S., Mohammadimehr, M. and Tounsi, A. (2019), "Nonlinear analysis of viscoelastic micro-composite beam with geometrical imperfection using FEM: MSGT electro-magneto-elastic bending, buckling and vibration solutions", *Struct. Eng. Mech.*, **71**(5), 485-502. https://doi.org/10.12989/sem.2019.71.5.485.

Batou, B., Nebab, M., Bennai, R., Atmane, H. A., Tounsi, A. and Bouremana, M. (2019), "Wave dispersion properties in imperfect sigmoid plates using various HSDTs", *Steel Compos. Struct.*, **33**(5), 699.https://doi.org/10.12989/scs.2019.33.5.699.

Bedia, W. A., Houari, M. S. A., Bessaim, A., Bousahla, A. A., Tounsi, A., Saeed, T. and Alhodaly, M. S. (2019), "A New Hyperbolic Two-Unknown Beam Model for Bending and Buckling Analysis of a Nonlocal Strain Gradient Nanobeams", *J. Nano Research*, **57**, 175-191. https://doi.org/10.4028/www.scientific.net/JNanoR.57.175.

Belbachir, N., Draich, K., Bousahla, A. A., Bourada, M., Tounsi, A. and Mohammadimehr, M. (2019), "Bending analysis of anti-symmetric cross-ply laminated plates under nonlinear thermal and mechanical loadings", *Steel Compos. Struct.*, **33**(1), 81-92. https://doi.org/10.12989/scs.2019.33.1.081.

Benchiha, A. and Madani, K. (2015), "Influence of the presence of defects on the stresses shear distribution in the adhesive layer for the single-lap bonded joint", *Struct. Eng. Mech.*, **53**(5), 1017-1030. https://doi.org/10.12989/sem.2015.53.5.1017.

Berghouti, H., Adda Bedia, E. A., Benkhedda, A. and Tounsi, A. (2019), "Vibration analysis of nonlocal porous nanobeams made of functionally graded material", *Adv. Nano Res.*, **7**(5), 351-364. https://doi.org/10.12989/anr.2019.7.5.351.

Boukhlif, Z., Bouremana, M., Bourada, F., Bousahla, A. A., Bourada, M., Tounsi, A. and Al-Osta, M. A. (2019), "A simple quasi-3D HSDT for the dynamics analysis of FG thick plate on elastic foundation", *Steel Compos. Struct.*, **31**(5), 503-516. https://doi.org/10.12989/scs.2019.31.5.503.

Boulefrakh, L., Hebali, H., Chikh, A., Bousahla, A. A., Tounsi, A. and Mahmoud, S. R. (2019), "The effect of parameters of visco-Pasternak foundation on the bending and vibration properties of a thick FG plate", *Geomech. Eng.*, **18**(2), 161-178. https://doi.org/10.12989/gae.2019.18.2.161.

Bourada, F., Bousahla, A. A., Bourada, M., Azzaz, A., Zinata, A. and Tounsi, A. (2019), "Dynamic investigation of porous functionally graded beam using a sinusoidal shear deformation theory", *Wind Struct.*, **28**(1), 19-30. https://doi.org/10.12989/was.2019.28.1.019.

Boutaleb, S., Benrahou, K. H., Bakora, A., Algarni, A., Bousahla, A. A., Tounsi, A., ... and Mahmoud, S. R. (2019), "Dynamic analysis of nanosize FG rectangular plates based on simple nonlocal quasi 3D HSDT", *Adv. Nano Res.*, **7**(3), 191. https://doi.org/10.12989/anr.2019.7.3.191.

Budhe, S., Banea, M.D., De Barros, S. and Da Silva, L.F.M. (2017), "An updated review of adhesively bonded joints in composite materials", *J. Adhesion Ahesives*, **72**, 30-42. https://doi.org/10.1016/j.ijadhadh.2016.10.010.

Chaabane, L. A., Bourada, F., Sekkal, M., Zerouati, S., Zaoui, F. Z., Tounsi, A., ... and Tounsi, A. (2019), "Analytical study of bending and free vibration responses of functionally graded beams resting on elastic foundation", *Struct. Eng. Mech.*, **71**(2), 185-196. https://doi.org/10.12989/sem.2019.71.2.185.

Cheuk, P.T. and Tong, L. (2002), "Failure of adhesive bonded composite lap shear joints with embedded precrack", *Compos. Sci. Technol.*, **62**(7-8), 1079-1095. https://doi.org/10.1016/S0266-3538(02)00054-4.

Daniel, I. M., Ishai, O., Daniel, I. M. and Daniel, I. (1994), *Engineering Mechanics of Composite Materials*, Oxford University \Press, New York, USA.

Delale, F., Erdogan, F. and Aydinoglu, M.N. (1981), "Stresses in adhesively bonded joints: a closed-form solution", *J. Compos. Mater.*, **15**(3), 249-271. https://doi.org/10.1177/002199838101500305.

Draiche, K., Bousahla, A. A., Tounsi, A., Alwabli, A. S., Tounsi, A. and Mahmoud, S.R. (2019), "Static analysis of laminated reinforced composite plates using a simple first-order shear deformation theory", *Comput. Concrete*, **24**(4), 369-378. https://doi.org/10.12989/cac.2019.24.4.369.

Draoui, A., Zidour, M., Tounsi, A. and Adim, B. (2019), "Static and Dynamic Behavior of Nanotubes-Reinforced Sandwich Plates Using (FSDT)", *J. Nano Res.*, **57**, 117-135. https://doi.org/10.4028/www.scientific.net/JNanoR.57.117.

Elhannani, M., Madani, K., Mokhtari, M., Touzain, S., Feaugas, X. and Cohendoz, S. (2016), "A new analytical approach for optimization design of adhesively bonded single-lap joint", *Struct. Eng. Mech.*, **59**(2), 313-326. https://doi.org/10.12989/sem.2-016.59.2.313.

Gulasik, H. and Coker, D. (2014), "Delamination-debond behaviour of composite T-joints in wind turbine blades", *J. Physics Conference Series, IOP Publishing*, *TORQUE 2014,* Denmark. https://iopscience.iop.org/issue/1742-6596/524/1.

Hellal, H., Bourada, M., Hebali, H., Bourada, F., Tounsi, A., Bousahla, A. A. and Mahmoud, S. R. (2019), "Dynamic and stability analysis of functionally graded material sandwich plates in hygro-thermal environment using a simple higher shear deformation theory", *J. Sandwich Struct. Mater.*, https://doi.org/10.1177/109-9636219845841.

Hussain, M., Naeem, M. N., Tounsi, A. and Taj, M. (2019), "Nonlocal effect on the vibration of armchair and zigzag SWCNTs with bending rigidity", *Adv. Nano Res.*, **7**(6), 431. https://doi.org/10.12989/anr.2019.7.6.431.

Irwin, G.R. (1957), "Analysis of stresses and strains near the end of a crack traversing a plate", *Appl. Mech*, **24**, 361-364.

Jayatilake, I. N., Karunasena, W. and Lokuge, W. (2016), "Finite element based dynamic analysis of multilayer fibre composite sandwich plates with interlayer delaminations", *Adv. Aircraft Spacecraft Sci.*, **3**(1), 15-28. https://doi.org/10.12989/aas.2016.3.1.015.

Jones, R.M. (2014), *Mechanics of Composite Materials*, CRC press, Florida, USA.

Kapidžić, Z., Nilsson, L. and Ansell, H. (2014), "Finite element modeling of mechanically fastened composite-aluminum joints in aircraft structures", *Compos. Struct.*, **109**, 198-210. https://doi.org/10.1016/j.compstruct.2013.10.056.

Karami, B., Janghorban, M. and Tounsi, A. (2019a), "Galerkin's approach for buckling analysis of functionally graded anisotropic nanoplates/different boundary conditions", *Eng. Comput.*, **35**(4), 1297-1316. https://doi.org/10.1007/s00366-018-0664-9.

Karami, B., Janghorban, M. and Tounsi, A. (2019b), "Wave propagation of functionally graded anisotropic nanoplates resting on Winkler-Pasternak foundation", *Struct. Eng. Mech.*, **70**(1), 55-66. https://doi.org/10.12989/sem.20-19.70.1.055.

Karami, B., Janghorban, M. and Tounsi, A. (2019c), "On exact wave propagation analysis of triclinic material using three-dimensional Bi-Helmholtz gradient plate model", *Struct. Eng. Mech.*, **69**(5), 487-497. https://doi.org/10.12989/sem.2019.69.5.487.

Karami, B., Janghorban, M. and Tounsi, A. (2019d), "On pre-stressed functionally graded anisotropic nanoshell in magnetic field", *J. Brazilian Soc. Mech. Sci. Eng.*, **41**(11), 495.

https://doi.org/10.1007/s40430-019-1996-0.

Karami, B., Shahsavari, D., Janghorban, M. and Tounsi, A. (2019e), "Resonance behavior of functionally graded polymer composite nanoplates reinforced with graphene nanoplatelets", *J. Mech. Sci.*, **156**, 94-105. https://doi.org/10.1016/j.ijmecsci.2019.03.036.

Khiloun, M., Bousahla, A. A., Kaci, A., Bessaim, A., Tounsi, A. and Mahmoud, S. R. (2019), "Analytical modeling of bending and vibration of thick advanced composite plates using a four-variable quasi 3D HSDT", *Eng. Comput.*, 1-15. https://doi.org/10.1007/s00366-019-00732-1.

Khiloun, M., Bousahla, A. A., Kaci, A., Bessaim, A., Tounsi, A. and Mahmoud, S. R. (2019), "Analytical modeling of bending and vibration of thick advanced composite plates using a four-variable quasi 3D HSDT", *Eng. Comput.*, 1-15. https://doi.org/10.1007/s00366-019-00732-1.

Li, H.C.H., Dharmawan, F., Herszberg, I. and John, S. (2006), "Fracture behaviour of composite maritime T-joints", *Compos. Struct.*, **75**(1-4), 339-350. https://doi.org/10.1016/j.compstruct.2006.04.052.

Li, W., Blunt, L. and Stout, K.J. (1997), "Analysis and design of adhesive-bonded tee joints", *J. Adhesion Ahesives*, **17**(4), 303-311. https://doi.org/10.1016/S0143-7496(97)00012-2.

Madenci, E. and Guven, I. (2015), *The Finite Element Method and Applications in Engineering Using ANSYS®*, Springer, Germany.

Mahieddine, A., Ouali, M. and Mazouz, A. (2015), "Modeling and simulation of partially delaminated composite beams", *Steel Compos. Struct.*, **18**(5), 1119-1127. https://doi.org/10.12989/scs.2015.18.5.1119.

Mahmoud, S. R. and Tounsi, A. (2019), "On the stability of isotropic and composite thick plates", *Steel Compos. Struct.*, **33**(4), 551-568. https://doi.org/10.12989/scs.2019.33.4.551.

Mahmoudi, A., Benyoucef, S., Tounsi, A., Benachour, A., Adda Bedia, E. A. and Mahmoud, S. R. (2019), "A refined quasi-3D shear deformation theory for thermo-mechanical behavior of functionally graded sandwich plates on elastic foundations", *J. Sandwich Struct. Mater.*, **21**(6), 1906-1929. https://doi.org/10.1177/1099636217727577.

Medani, M., Benahmed, A., Zidour, M., Heireche, H., Tounsi, A., Bousahla, A. A., ... and Mahmoud, S. R. (2019), "Static and dynamic behavior of (FG-CNT) reinforced porous sandwich plate using energy principle", *Steel Compos. Struct.*, **32**(5), 595-610. https://doi.org/10.12989/scs.2019.32.5.595.

Meksi, R., Benyoucef, S., Mahmoudi, A., Tounsi, A., Adda Bedia, E. A. and Mahmoud, S. R. (2019), "An analytical solution for bending, buckling and vibration responses of FGM sandwich plates", *J. Sandwich Struct. Mater.*, **21**(2), 727-757. https://doi.org/10.1177/1099636217698443.

Mishra, P.K., Pradhan, A.K. and Pandit, M.K. (2016), "Delamination propagation analyses of spar wing-skin joints made with curved laminated FRP composite panels", *J. Adhesion Sci. Technol.*, **30**(7), 708-728. https://doi.org/10.1080/01694243.2015.1121851.

Mokhtari, M., Shahravi, M. and Zabihpoor, M. (2017), "Development of dynamic behavior of the novel composite T–Joints: numerical and experimental", *Adv. Aircr. Space. Sci*, **5**, 385-400. https://doi.org/10.12989/aas.2018.5.3.385.

Nimje, S.V. and Panigrahi, S.K. (2015), "Interfacial failure analysis of functionally graded adhesively bonded double supported tee joint of laminated FRP composite plates", *J. Adhesion Ahesives*, **58**, 70-79. https://doi.org/10.1016/j.ijadhadh.2015.01.002.

Panigrahi, S.K. and Pradhan, B. (2007), "Three dimensional failure analysis and damage propagation behavior of adhesively bonded single lap joints in laminated FRP composites", *J. Reinforced Plastics Compos.*, **26**(2), 183-201. https://doi.org/10.1177/0731684407070026.

Perić, M., Tonković, Z., Rodić, A., Surjak, M., Garašić, I., Boras, I. and Švaić, S. (2014), "Numerical analysis and experimental investigation of welding residual stresses and distortions in a T-joint fillet weld", *Mater. Design*, **53**, 1052-1063. https://doi.org/10.1016/j.matdes.2013.08.011.

Prashob, P. S., Shashikala, A. P. and Somasundaran, T. P. (2017a), "Behaviour of carbon fiber reinforced polymer strengthened tubular joints", *Steel Compos. Struct.*, **24**(4), 383-390. https://doi.org/10.12989/scs.2017.24.4.383.

Prashob, P. S., Shashikala, A. P. and Somasundaran, T. P. (2017b), "Review of existing techniques and fibre reinforced polymers used for strengthening tubular joints", *Struct. Monitor. Maintenance*, **4**(3),255-268. https://doi.org/10.12989/smm.2017.4.3.255.

Rybicki, E.F. and Kanninen, M.F. (1977), "A finite element calculation of stress intensity factors by a modified crack closure integral", *Eng. Fracture Mech.*, **9**(4), 931-938. https://doi.org/10.1016/0013-7944(77)90013-3.

Sahla, M., Saidi, H., Draiche, K., Bousahla, A. A., Bourada, F. and Tounsi, A. (2019), "Free vibration analysis of angle-ply laminated composite and soft core sandwich plates", *Steel Compos. Struct.*, **33**(5), 663.https://doi.org/10.12989/scs.2019.33.5.663.

Semmah, A., Heireche, H., Bousahla, A. A. and Tounsi, A. (2019), "Thermal buckling analysis of SWBNNT on Winkler foundation by non-local FSDT", *Adv. Nano Res.*, **7**(2), 89. https://doi.org/10.12989/anr.2019.7.2.089.

Tsai, S. (2018), Introduction to composite materials, Routledge.

Vosoughi, A. R. (2015), "A developed hybrid method for crack identification of beams", *Smart Struct. Syst.*, **16**(3), 401-414. https://doi.org/10.12989/sss.2015.16.3.401.

Xie, D., Waas, A.M., Shahwan, K.W., Schroeder, J.A. and Boeman, R.G. (2004), "Computation of energy release rates for kinking cracks based on virtual crack closure technique", *Comput. Modell. Eng. Sci.*, **6**(6), 515-524. https://pdfs.semanticscholar.org/2792/8c5f43f3814c404d56f6403 4b4f15ad644cc.

Zaoui, F. Z., Ouinas, D. and Tounsi, A. (2019), "New 2D and quasi-3D shear deformation theories for free vibration of functionally graded plates on elastic foundations", *Compos. Part B Eng.*, **159**, 231-247. https://doi.org/10.1016/j.compositesb.2018.09.051.

Zarga, D., Tounsi, A., Bousahla, A. A., Bourada, F. and Mahmoud, S. R. (2019), "Thermomechanical bending study for functionally graded sandwich plates using a simple quasi-3D shear deformation theory", *Steel Compos. Struct.*, **32**(3), 389-410. https://doi.org/10.12989/scs.2019.32.3.389.

CC